

SPECTRAL PHASE MODULATION AND CHIRPED PULSE AMPLIFICATION IN HIGH GAIN HARMONIC GENERATION

Z. Wu, H. Loos, Y. Shen, B. Sheehy, E. D. Johnson, S. Krinsky, J. B. Murphy, J. Rose, T. Shaftan, X.-J. Wang, L. H. Yu, NSLS, Brookhaven National Laboratory, Upton NY, USA 11973

Abstract

Amplitude and phase measurements are conducted on the 266 nm output of the DUVFEL laser at the National Synchrotron Light Source (NSLS) at Brookhaven National Laboratory. With the FEL operating in High Gain Harmonic Generation (HGHG) mode, we have studied narrow-bandwidth HGHG output, and observe pulses near the transform limit. We have also chirped both the electron bunch energy and the seed pulse wavelength, and successfully imposed a linear chirp on the HGHG output. These results demonstrate the potential to generate short harmonic pulses through chirped pulse amplification [1] or coherently shape FEL output.

INTRODUCTION

In High Gain Harmonic Generation [2] operation of an FEL, a coherent optical seed pulse at a subharmonic of the resonant FEL output wavelength is used to impose a coherent microbunching of the electron bunch before it enters the radiator. This permits rapid saturation of the harmonic output over short distances, and the possibility of reaching X-ray wavelengths by cascading the process through a relatively small number of stages [3].

An important advantage of this scheme is the longitudinal coherence of the harmonic output. Longitudinal coherence in itself is important for many experimental applications of short pulse X-rays, but it also presents the possibility of achieving femtosecond pulses through chirped pulse amplification (CPA) [1], and shaping short-wavelength pulses on ultrafast time scales.

Pulse-shaping techniques developed for ultrafast laser systems allow complex modulations limited essentially only by the available bandwidth of the pulse. Manipulating optical interactions with such pulses yields unprecedented control over dynamics, and such ‘quantum control’ been demonstrated in a multitude of systems [4]. In principle, such techniques could be extended all the way down to X-ray wavelengths by seeding an HGHG cascade with a shaped seed pulse. The question then becomes what role noise or distortion introduced by HGHG will have on the shaping capabilities. For this reason, it is useful to consider the full ‘HGHG transfer function’, and measure both the amplitude and phase of the output pulse as a function of the modulation of the seed pulse. This should also have an added benefit as an FEL diagnostic, since modulations introduced by HGHG are likely to be sensitive functions of electron bunch characteristics and radiator dynamics.

In this work, we study the simplest pulse shape: a linear frequency chirp. This is an important test of the feasibility of CPA. If a linear chirp can be imposed on the HGHG

output, a dispersive line could compress it to pulse widths much shorter than the electron bunch length. A theoretical study of this process predicts achievable pulse widths of 4 fsec in X-ray FELs [1]. We demonstrate amplitude and phase measurements of HGHG, using spectral phase interferometry for direct electric field reconstruction (SPIDER) [5]. This is the first time that SPIDER has been reported for wavelengths this short. We examine first the narrow bandwidth emission produced by HGHG using an unchirped electron bunch, and a nearly-monochromatic seed. We then chirp both the frequency of the seed pulse and the energy of the electron bunch, and measure the chirp imposed on the HGHG output. Finally we discuss the implication for effective pulse compression.

EXPERIMENTAL SETUP

SPIDER

The SPIDER technique, developed by Walmsley and coworkers [5], is an interferometric technique for recovering the amplitude and phase of an ultrafast pulse. Its principal advantages in FEL applications are that a well-characterized reference pulse is not needed, and a rapid inversion algorithm that makes shot to shot measurements possible. We use a variant here known as down-conversion SPIDER [6]. A diagram of our implementation of the technique is shown in Fig. 1. Light from the seed pulse at 800 nm is separated from the 266 nm HGHG output and stretched in a grating compressor to a pulse width of 55 psec FWHM, to serve as the shearing pulse. The 266 nm pulse passes through a Michelson interferometer, which splits it into two

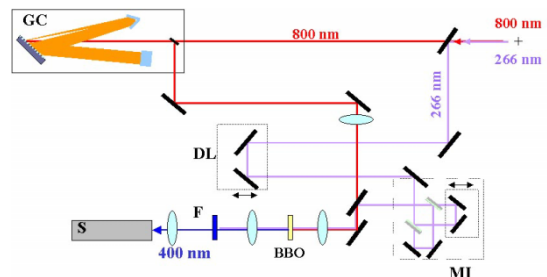


Fig 1. SPIDER implementation for measurement of 266 nm HGHG pulses. GC, grating compressor; DL, delay line; MI, Michelson interferometer, BBO, crystal for down-conversion; F, filter, S, spectrometer. For calibration, the 800 nm beam is blocked and filter F is removed.

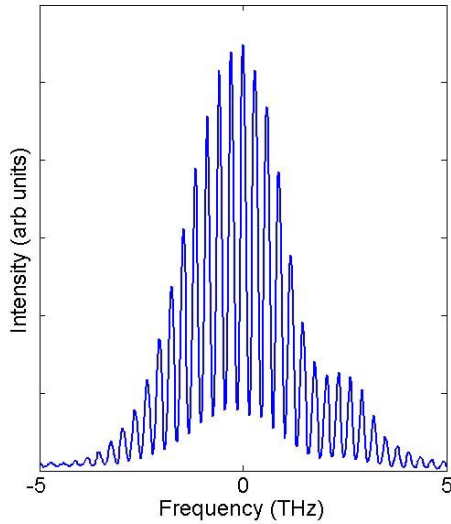


Fig. 2 SPIDER trace from a chirped HGHG pulse.

identical replicas with a delay of $\tau = 3.5$ psec between them. Both 266 nm replicas are mixed with the chirped shearing pulse in a 250 μm thick BBO crystal, which is phase-matched for down-conversion to 400 nm ($\theta=44.7$ deg. Type I). They each see a nearly monochromatic slice of the long shearing pulse, with a frequency difference $\Omega = \tau\beta_{\text{ref}} = 0.2$ THz, where $\beta_{\text{ref}} = 0.06$ THz/psec is the frequency chirp of the shearing pulse. The two 400 nm replicas produced in the down-conversion are thus shifted in frequency by Ω and, as phase is preserved in the down-conversion, a frequency component ω in one of the replicas carries the same phase information from the parent pulse as the $\omega+\Omega$ component in the other replica. Hence by interfering the two pulses, the phase difference between $(\omega, \omega+\Omega)$ frequency pairs may be measured and the spectral phase variation over the entire pulse determined.

Fig. 2 shows a SPIDER interferogram trace. In the absence of the spectral shear ($\Omega=0$), the fringe spacing would be just $1/\tau$. The phase variation across the pulse spectrum is manifested in variations from this spacing. Abstracting this “carrier phase” from the measurement is a recurring problem in spectral interferometry, of which SPIDER is a special case. Dorrer [7] notes that such measurements are very sensitive to calibration errors in the spectrometer, and that this problem is often avoided in SPIDER by generating a calibration with $\Omega=0$, while maintaining a spectrometer configuration identical to that used in the measurement. The effect of the spectrometer error is then largely canceled by subtraction of the calibration from the measurement. He also notes, and it has been experimentally demonstrated [6] that, if the ratio of parent and converted pulse wavelengths is an integer, then an identical spectrometer configuration can be maintained by using different grating orders for the

calibration and the measurement. In fact, a slightly less restrictive condition holds: if these wavelengths are both harmonics of a third wavelength, the same can be done. Thus, here we set the spectrometer (a 320 mm focal length Jobin-Yvon TRIAX, using a 2400 line/mm grating) to a center wavelength of 800 nm, and measure the 400 nm SPIDER trace in second order. The calibration is made by interfering the 266 nm parent pulses directly, and measuring in third order.

For the inversion, we follow the procedure of Iaconis and Walmsley [8] to obtain the phase. The spider trace is fourier-transformed, filtered with a fourth-order supergaussian centered at $t = \tau$, with a $1/e$ half-width of 1.5 psec, and back-transformed to the frequency domain. This phase is unwrapped, the calibration phase subtracted, and the result concatenated to obtain the spectral phase of the test pulse. The amplitude is obtained from a similar procedure [9], using the $t = 0$ component of the transformed SPIDER trace. With the field fully specified in the frequency domain, the temporal profile, frequency chirp, etc, can be obtained after transforming into the time domain.

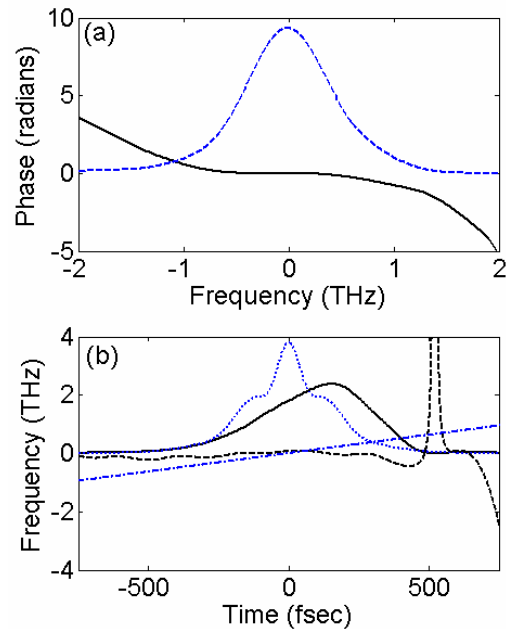


Fig. 3 Spectral and temporal characteristics of an unchirped HGHG pulse, retrieved from SPIDER. Intensity profiles are plotted in arbitrary units. (a) Spectral intensity (dashed), spectral phase (solid). (b) instantaneous frequency (dashed), 3 times the residual frequency chirp of the 6 psec seed laser (dash-dot), intensity (solid), transform limited intensity (phases set to zero, dotted line)

HGHG

The Brookhaven DUVFEL operation in HGHG mode is fully described elsewhere [10]. A 170 MeV, 300 pC electron bunch is generated using a BNL GUN-IV

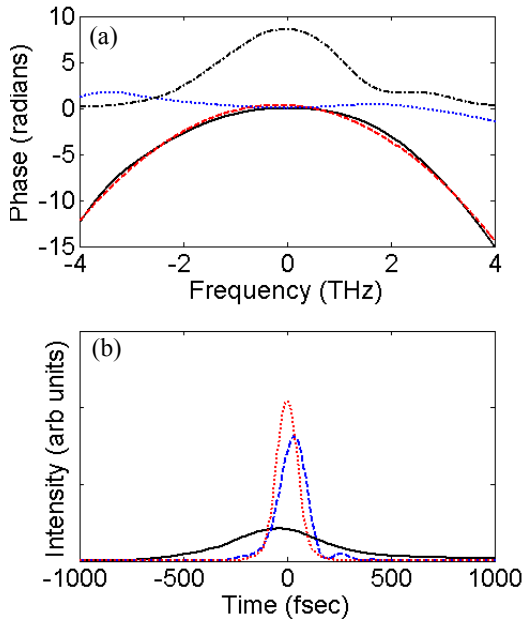


Fig. 4 Spectral and temporal characteristics of a chirped HGHG pulse, retrieved from SPIDER. (a) Spectral intensity (dash-dot), spectral phase (solid), 2nd order polynomial fit to spectral phase (dashed), spectral phase with quadratic component subtracted (dotted). (b) intensity profile (solid), intensity with quadratic phase component subtracted (dashed), transform-limited intensity (dotted)

photoinjector followed by a 4-stage linear accelerator. A magnetic chicane compressor after the first two linac stages permits the compression of the electron bunch down to ~ 1 psec FWHM. Varying the phase of the third and fourth linac stages permits the imposition of an energy chirp on the bunch. Following the linac, the electron bunch energy is modulated using a synchronized optical seed pulse in a 1-meter undulator, which is resonant at the seed pulse wavelength of 800 nm. The seed pulse is derived from the same laser that drives the photoinjector, and its chirp is adjusted by varying its length in a grating compressor. Following a dispersive section, the coherently microbunched beam enters the 10-m NISUS wiggler, which is resonant at the third harmonic of the seed. Both the 266 nm third-harmonic HGHG output and the 800 nm seed propagate to the SPIDER set-up shown in Fig 1.

RESULTS AND DISCUSSION

We first examine narrow bandwidth HGHG (0.12% relative bandwidth rms), with no chirp. For this, the seed pulse was stretched to 6 psec in length (FWHM), and the electron beam parameters were optimized to minimize the HGHG bandwidth. Fig. 3 shows typical data, obtained from SPIDER from a single HGHG shot. In the first panel the spectrum and spectral phase variation are shown. The second panel shows the temporal profile of the pulse obtained by Fourier-transforming the data in the first panel, as well the instantaneous frequency of the pulse as a function of time. The center frequency is subtracted for clarity. The frequency is essentially flat over the length of the pulse, with some distortion towards the trailing end and in the wings. The chirp of the seed pulse, multiplied by the harmonic number $n=3$ of the HGHG process, is shown for reference. Because the electron beam is not chirped, we do not expect to see the chirp reflected in the HGHG output.

The flat phase profile indicates that the pulse is nearly transform-limited. The pulse shape does deviate significantly from a Gaussian though. The time bandwidth product is $\sigma_\omega\sigma_\tau = 0.9$, or 1.8 times the transform limit for a Gaussian pulse. However, if we set the spectral phase identically to zero, and take the calculated temporal profile as the transform limit, then the width (rms) of the measured profile is only 20 % larger than the transform-limited width, $\sigma_\tau/\sigma_{\tau TL} = 1.2$. For a 50 shot sample, we obtain $\sigma_\omega\sigma_\tau = 1.15 \pm 0.15$ and $\sigma_\tau/\sigma_{\tau TL} = 1.4 \pm 0.1$.

In order to obtain a chirped HGHG pulse, it is necessary to chirp the energy of the electron bunch so that the resonant frequency at each point along the bunch is equal to the third harmonic of the instantaneous seed frequency, i.e., the resonant frequency chirp must be 3 times that of the seed pulse. This is done by running the

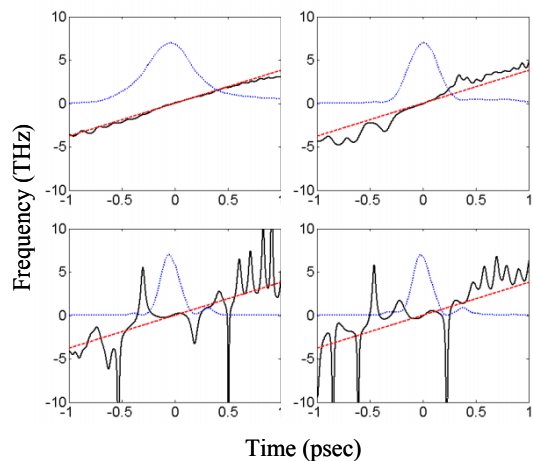


Fig. 5 Time-dependent frequency for several chirped HGHG pulses. The data in the first panel are for the shot represented in Fig 4. The curves are instantaneous frequency (solid), theoretical chirp (dashed, see text), and the intensity profile (dotted)

third and fourth linac tanks off-crest, and incompletely compensating the chirp imposed for bunch compression

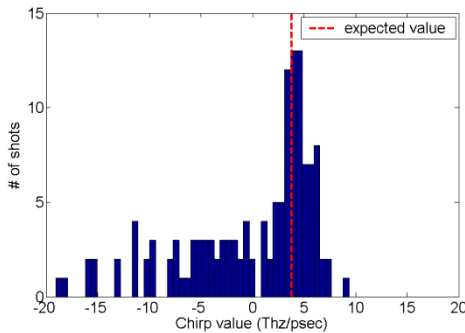


Fig. 6 Distribution of frequency chirp values measured in a 200 fsec window around the center of a set of 136 HGHG pulses. The dashed line indicates the chirp expected to be imposed by the chirped seed pulse

(using both tanks reduces the effect of rf curvature).

Due to technical problems during the experimental run, we were only able to match the electron and seed chirps to within 40%. The 800 nm seed pulse is 2 psec long FWHM, with a bandwidth of 5.4 nm FWHM, and a chirp of 1.27 THz/psec. The corresponding chirp to be imposed on the HGHG output is then $\beta_{266} = 3.8$ THz/psec, but the energy chirp imposed on the electron bunch corresponded to a resonant frequency chirp of only 2.7 THz/psec. We find however, that the seed chirp is still clearly observable in the HGHG output.

Fig. 4 shows the recovered spectrum, phase and temporal information for a single shot. A parabolic spectral phase indicates a linear frequency chirp. Panel (a) shows the spectrum, the spectral phase, a parabolic fit to the phase, and the resultant phase when the quadratic component of the phase is subtracted off. Panel (b) shows the temporal profile as measured, the transform-limited profile (obtained by setting the spectral phase identically to zero), and the temporal profile that would obtain if the quadratic part of the phase were removed. The latter is to simulate the temporal profile expected after putting the pulse through the appropriate compressor. We define the compression ratio as the ratio of the as-measured rms pulse width to the rms pulse width of this distribution.

The instantaneous frequency may be defined as the first derivative of the temporal phase, and the chirp is then the second derivative. Both may be obtained from the data, and the frequency vs time is displayed for several shots, along with their respective temporal profiles, in Fig. 5. The center frequency is subtracted for clarity, and the theoretical curve represents a constant chirp of 3 times the seed pulse chirp. The first shot displayed in Fig. 5 is for the same shot represented in Fig. 4., and shows a near-constant chirp over the length of the pulse. The compression ratio for this pulse is 3.2, and, as is clear

from Fig. 4(b), the compressed pulse would be close to the transform limit. More typical shots are shown in the subsequent panels. The strong phase variation in the wings destroys the compressibility for most of the pulses, but a chirp near the expected value is usually observed near the peak of the pulse. If we simulate a single compressor for all pulses by extracting the same quadratic component from the phase as for the shot in Fig 4, we find that, for 136 pulses measured, 20, or 15%, would show some compression. However, if we fit the chirp in a 200 fsec window about the peak of the pulse we find that the distribution of chirp values (Fig. 6) is peaked about the expected value β_{266} .

The shot-to-shot fluctuations in compressibility probably arise from a combination of the mismatch of electron bunch and optical seed chirps, the 150 fsec (rms) synchronization jitter between the electron bunch and seed pulse, and fluctuations in the electron bunch compression that were due to technical problems during the experiment. The latter two, coupled with the nonlinearity of the electron bunch chirp due to rf curvature, can lead to emission effectively occurring over only a fraction of the electron bunch. Supporting this interpretation is a strong positive correlation observed between the pulse width of the HGHG pulse and the compression ratio.

While the control of these factors will be necessary for a practical implementation of chirped pulse amplification in high gain harmonic generation FEL systems, the observation of compressible pulses in the present work, does demonstrate the viability of the technique, and the potential for more complex shaping at short wavelengths.

ACKNOWLEDGEMENTS

The work was performed under DOE contract DE-AC02-98CH10886.

REFERENCES

- [1] L. H. Yu, E. Johnson, D. Li, and D. Umstadter Phys. Rev. E **49**, 4480-4486 (1994)
- [2] L. H. Yu Phys. Rev. A **44**, 5178-5193 (1991); L. H. Yu et al. Phys. Rev. Lett. **91**, 074801 (2003);
- [3] L. H. Yu, in Proceedings of the X-Ray FEL Theory and Simulation Codes Workshop SLAC Stanford University Sep 23-24, (1999)
- [4] For a recent review, see D. Goswami, Phys. Rep. **374**, 385-481 (2003)
- [5] C. Iaconis and I. A. Walmsley, Opt. Lett. **23**, 792-794 (1998).
- [6] P. Londero et al J. Mod. Opt. **50**, 179 (2003)
- [7] C. Dorrer. J. Opt. Soc. Am **B 16**, 1160-1168 (1999).
- [8] C. Iaconis and I. A. Walmsley, IEEE J. Quant. Elect.. **35**, 501 (1999)
- [9] A. Muller and M. Laubscher, Opt. Lett. **26**, 1915 (2001).
- [10] A. Doyuran et al Phys Rev ST AB **7**, 050701, (2004)